To appear in JASTP, 2001

Long term studies of equatorial spread *F* using the JULIA radar at Jicamarca

D. L. Hysell and J. D. Burcham

Dept. of Physics and Astronomy, Clemson University, Clemson, South Carolina

Abstract.
JULIA radar observations of equatorial spread *F* (ESF) plasma irregularities made between August, 1996 and April, 2000 are analyzed statistically. Interpretation of the data is simplified by adopting a taxonomy of echo types which distinguishes between bottom-type, bottomside, topside, and post-midnight irregularities. The data reveal patterns in the occurrence of ESF in the Peruvian sector that are functions of season, solar flux, and geomagnetic activity. We confirm earlier work by *Fejer et al.* [1999] showing that the quiet-time climatology of the irregularities is strongly influenced by the climatology of the zonal ionospheric electric field. Under magnetically quiet conditions, increasing solar flux implies greater prereversal enhancement amplitudes and, consequently, irregularity appearances at earlier times, higher initial altitudes, and higher peak altitudes. Since the post-reversal westward background electric field also grows stronger with increasing solar flux, spread *F* events also decay earlier in solar maximum than in solar minimum. Variation in ESF occurrence during geomagnetically active periods is consistent with systematic variations in the electric field associated with the disturbance dynamo and prompt penetration described by *Fejer and Scherliess* [1997] and *Scherliess and Fejer* [1997]. Quiet-time variability in the zonal electric field contributes significantly to variability in ESF occurrence. However, no correlation is found between the occurrence of strong ESF and the time history of the zonal electric field prior to sunset.

1. Introduction

The JULIA (Jicamarca Unattended Long term investigations of the Ionosphere and Atmosphere) radar is a PC-based data acquisition system that uses low power transmitters and the Jicamarca main antenna and functions as an MST or as a coherent scatter radar. Between August, 1996 and April, 2000, the JULIA radar was used to probe *E* and *F* region plasma irregularities over 24 hour periods on nearly 300 days when other Jicamarca activities did not take precedence. Observations were made over different seasons, solar flux levels, and geomagnetic conditions. The primary operating mode measured backscatter signal-to-noise ratios, first moment Doppler velocities, and interferometric zonal drift speeds between 95 and about 900 km altitude. Details of the investigation have been presented by *Hysell and Burcham* [1998]. Processed data can be viewed using the web server at `http://landau.geo.cornell.edu`.

This paper addresses trends in the overall occurrence of *F* region irregularities rather than characteristics of isolated events. While the echoes in our dataset exhibit considerable morphological variability, clear patterns in their occurrence are apparent. These patterns become more evident when the echoes are categorized into a few distinct types. While no two spread *F* events appear exactly alike in the radar data, most events fall naturally into categories and evolve according to one of a few scripts.

In order to demonstrate skill, forecasts of ESF must outperform predictions derived from climatological or persistence models. This paper presents the climatological record of ESF occurrence versus season and solar flux level, evaluates the effects of geomagnetic activity on the occurrence of spread *F*, and analyzes the persistence. We argue that the climatological behavior of the zonal electric field, itself controlled by the neutral wind behavior, plays a predominant role in controlling the climatology of spread *F*. We show that the effects of geomagnetic activity on ESF are mainly consistent with the behavior of the disturbance dynamo and of prompt penetration as described by *Fejer and Scherliess* [1997] and *Scherliess and Fejer* [1997]. Finally, we discuss the effects of quiet-time electric field variability on the day-to-day variability of spread *F*. A better understanding of this variability is prerequisite for developing skillful forecast models.

2. Echo types

Coherent scatter radar observations of ionospheric plasma irregularities are conventionally displayed in range time intensity (RTI) format in which backscatter power is plotted against altitude and time. Many years of spread *F* investigations carried out at Jicamarca and elsewhere have led to the accumulation and dissemination of large numbers of RTI plots known for their complexity and variability. These RTI plots may convey an exaggerated sense of the "randomness" of equatorial spread *F*, however. Although they have two dimensions, RTI plots should not be interpreted as two-dimensional spatial representations of the irregularities except perhaps for very broad features. This is because the velocity with which the irregularities drift past the radar is neither uniform nor constant, because the eddy turnover time for dominant features in the disturbed ionospheric flow is less than the time it takes to generate an RTI map, and because the beamwidth of even the Jicamarca antenna is broad compared to the size of the primary plasma waves involved in spread *F*. We believe that much of the structure apparent in RTI plots is due to a complicated instrument function and should be ignored. RTI plots from the JULIA dataset exhibit clear patterns when interpreted simply as indications of at what altitudes and times irregularities occur.

As argued by *Hysell and Burcham* [1998], most of the echoes observed with the JULIA radar fall neatly into a few main categories. These are bottom-type layers, bottomside layers, topside layers (radar plumes), and post midnight irregularities. Representative examples of these types are shown in Figure 1. In this figure, three examples of each type observed at different phases of the solar cycle are shown.

The characteristics of bottom-type, bottomside, and topside layers were summarized by *Hysell* [2000]. All are manifestations of ionospheric interchange instabilities. Bottom-type layers appear to be the signatures of primary waves with scale sizes transverse to **B** smaller than about 1 km. They can exist at low altitudes on flux tubes with *E* region dominated integrated conductivities without coupling to the *E* region and electrically "shorting out". These narrow layers mainly drift westward under control of the *E* region dynamo, even during solar maximum, and cannot exhibit much vertical development. Bottomside layers meanwhile represent interchange instabilities existing at higher altitudes or later times on flux tubes imposing no significant *E* region loading. They are also mainly confined to the linearly unstable bottomside but drift eastward, exhibit significant vertical development, and can penetrate the *F* peak, occasionally launching narrow channels of depleted plasma into the topside. Bottomside layers have primary waves with transverse scale sizes of a few km that resemble the irregularities emerging in numerical simulations of interchange instabilities initialized by broad-band, random noise. Finally, topside layers or radar plumes represent large-scale, deep plasma depletions that break through to the topside and ascend rapidly to high altitudes. Radar plumes accompany what appear to be drastic deformations of the bottomside *F* layer and resemble the wedge-shaped depletions that emerge in numerical simulations initialized by large-scale, large amplitude perturbations (e.g. *Zargham* [1988]).

Figure 1 illustrates how bottom-type layers vary with solar activity. The altitude at which layers typically appeared increased from about 200 km to about 400 km with an increase in the 10.7 cm flux from 70 to 200. Whereas the layers sometimes persist until local midnight during solar minimum, they typically vanished by 22 LT at solar maximum. Once bottom-type layers disappear on a given evening, they seldom reappear. The morphology of radar plumes is also affected by changing solar flux. As solar flux increases, plumes tend to form earlier in the evening and at higher altitude, to achieve higher maximum altitudes, to cross through the radar scattering volume more rapidly, and to desist earlier.

Figure 1 depicts bottom-type, bottomside, and topside irregularities occurring by themselves. However, different layer types occur sequentially, following a routine choreography. Bottom-type layers generally emerge first, soon after sunset. Often, they descend under the influence of a westward zonal electric field until the underlying plasma waves are stabilized by collisions. Should they instead ascend for a time, radar plumes often appear over the radar shortly after the bottom-type layer reaches its apex. More radar plumes may follow. Eventually, bottomside layers remain and can be observed until about local midnight. This is the common ordering of events. On a given evening, steps can be skipped, but the order is usually followed.

Table 1. presents overall occurrence statistics sorted by the 10.7 cm solar flux index. The echo type refers to strongest type of echo occurring on a given evening prior

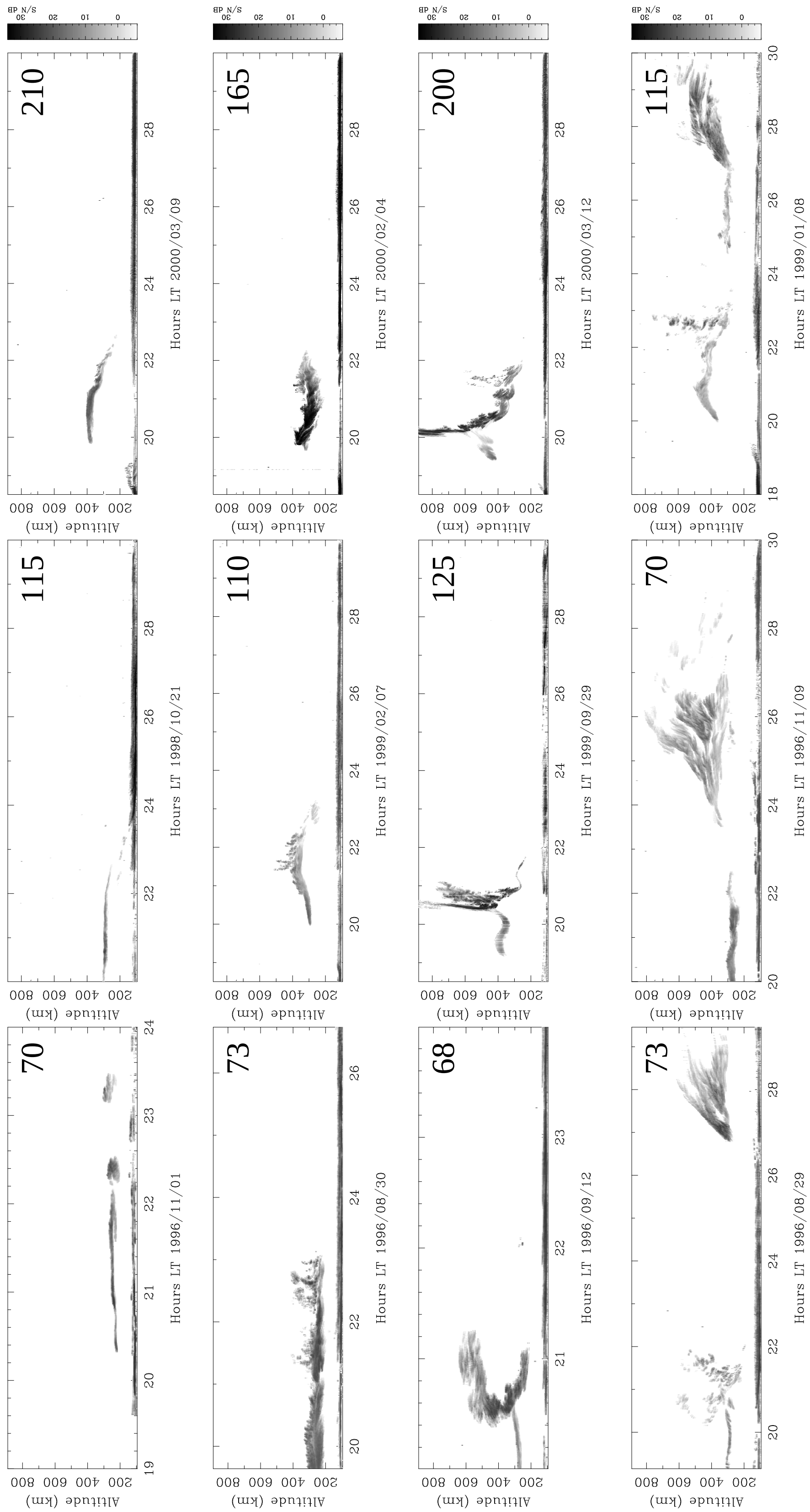

Figure 1. RTI plots depicting groups of bottom-type layers (first row), bottomside layers (second), radar plumes (third), and post-midnight irregularities (fourth). Representative 10.7 cm solar flux levels are indicated on the upper right of each plot. Note that the plots do not all start and end at the same times.

Table 1. Occurrence statistics for echo types versus 10.7 cm solar flux.

	$\phi < 90$	$90 < \phi < 160$	$160 < \phi$
none	12%	16%	10%
bottom-type	23%	27%	31%
bottomside	15%	19%	16%
topside	50%	38%	43%

to local midnight, ranked from the weakest (none) to the strongest (topside). (Note that the actual strength of the echoes themselves has little to do with season or solar cycle.) The table represents results from all seasons except June solstice but, like our database, is strongly influenced by equinox conditions. Our seasonal coverage undoubtedly affects the statistics. Occurrences of irregularities during June solstice are rare. The statistics shown here do not exhibit significant solar cycle variations except perhaps for a small increase in the occurrence of topside plumes during solar minimum.

Finally, the JULIA radar has detected many instances of irregularities forming well after local midnight. Three representative examples of post-midnight irregularities are shown in Figure 1. These irregularities do not follow the bottom-type topside bottomside ordering but instead have a distinctly different morphology. In RTI diagrams, post-midnight irregularities give rise to characteristic wedge shapes. As a rule, they occur following periods of geomagnetic activity and are most common in solar minimum (see below). They are observed during solar maximum following major storms.

3. Climatology

Figure 2 and Figure 3 present the occurrence statistics of JULIA spread *F* echoes for equinox and December solstice conditions, respectively. The upper, middle, and lower rows in each case correspond to low, moderate, and high solar flux conditions. Geomagnetically quiet and active conditions are depicted in the left and right columns, respectively (see below). The graphs themselves represent the percentage rate of occurrence of detectable echoes binned in altitude and local time. Histograms at the bottom of each grayscale plot show the number of datasets contributing to the statistics. More data were taken during magnetically quiet than active periods, and the shortage of data from disturbed solstice conditions in particular renders those results inaccurate. Solid lines superimposed on the quiet-time plots show quiet time average vertical plasma drifts derived from incoherent scatter measurements [*Scherliess and Fejer*, 1999].

The echo phenomenology depicted here will be seen to support many of the conclusions drawn recently by *Fejer et al.* [1999], who demonstrated that the quiet-time climatology of *F* region irregularities observed in the Peruvian sector is closely tied to the quiet-time climatology of the zonal ionospheric electric field. The likelihood of observing irregularities in a given season and year, they found, depends mainly on the average amplitude of the prereversal enhancement, time of the evening reversal, and post reversal field strength. The climatology of the electric field meanwhile is controlled by the behavior of the neutral winds and the distribution of conductivity along the magnetic flux tubes and already has been well established [*Scherliess and Fejer*, 1999].

The zonal electric field affects postsunset *F* region stability mainly in two ways. An eastward (westward) field drives a zeroth-order Pedersen current that is directly and immediately destabilizing (stabilizing). More importantly, an eastward field causes the *F* layer to ascend over time to altitudes where ion-neutral collisions are less frequent and the linear growth rate of the Rayleigh Taylor instability is higher and less influenced relatively by the ultimate direction of the electric field. Climatological changes in the behavior of the electric field should affect the climatology of ESF occurrence accordingly.

Figures 2 and 3 support the findings of *Fejer et al.* [1999] in showing that, under magnetically quiet conditions, the effect of increasing solar flux is to cause irregularities to occur earlier and at higher altitudes and to penetrate to much higher topside altitudes on average. This is consistent with the increase in both amplitude of the prereversal enhancement and the time of the evening reversal of the zonal electric field associated with increasing solar flux. Furthermore, since the average post reversal westward electric field also grows stronger with increasing solar flux, spread *F* events tend to vanish earlier in solar maximum than in solar minimum. The late reversal time and small post-reversal electric fields associated with low flux December solstice in particular lead to long-lived spread *F* events. Post-midnight spread *F* is likewise observed most frequently during solar minimum, when the small post-reversal zonal electric field can most easily be overcome by storm-driven electric fields (see below).

4. Persistence

For a meteorological forecast to demonstrate skill, it must outperform both climatological forecast models and models based on persistence, the forward extrapolation of current conditions. The climatology of ESF irregularities was de-

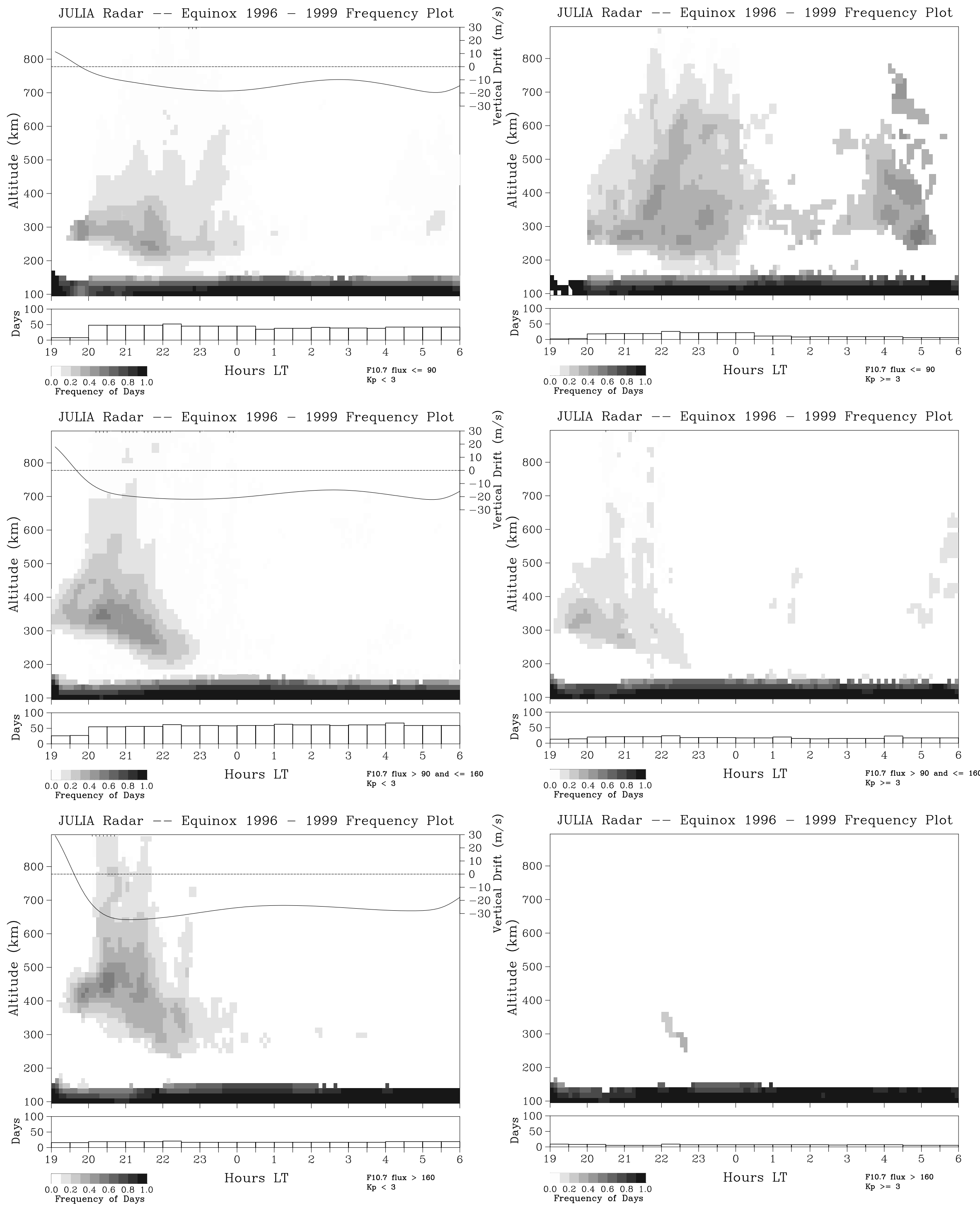

Figure 2. Binned JULIA data showing the occurrence statistics of radar echoes for different solar flux and geomagnetic activity levels during equinox (Feb – Apr, Aug – Oct). Grayscales depict the likelihood of detecting echoes in bins 6 min. wide by 15 km in altitude. Geomagnetic activity is based on the Kp index averaged over the preceding 6 hours. Note that relatively few datasets corresponding to solar maximum magnetically disturbed conditions have thus far been taken.

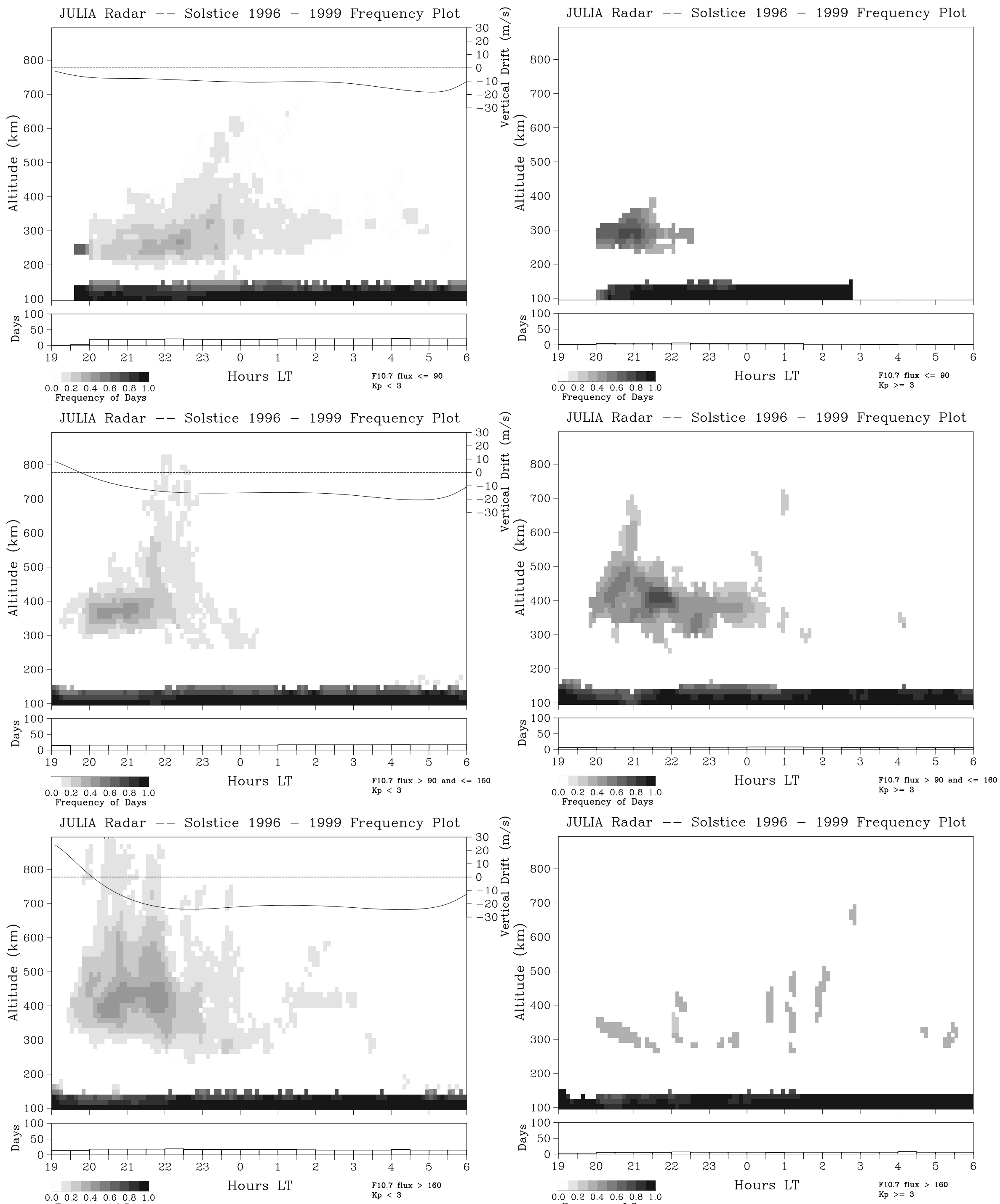

Figure 3. Same as previous figure except for December solstice (Nov – Jan). Note that very few data corresponding to geomagnetically active conditions have so far been collected.

scribed in the preceding section. Here, we apply the concept of persistence to the irregularities and examine the correlation in the day-to-day occurrence of radar plumes. A quick survey of all the JULIA data suggests a tendency for radar plumes to occur over consecutive days separated by days of inactivity. A similar phenomenon is apparent in satellite-based spread *F* databases such as the AE-E dataset (R. Heelis, personal communication, 2000).

We can define a random variable with two states representing the daily pre-midnight occurrence or non-occurrence of a topside radar plume in the JULIA dataset. The random variable will have a different mean and variance for different seasons and phases of the solar cycle. Using standard techniques and definitions, we can compute the normalized autocorrelation function of this random variable for different lags, where the lags are integer numbers of days. Autocorrelation values approaching unity would indicate a strong tendency for ionospheric conditions to repeat night after night.

Table 2. Correlation analysis of plume occurrence.

F10.7 Index	Persistence (n) Equinox	Persistence (n) All seasons
$\phi < 80$	0.38 (66)	0.33 (70)
$80 < \phi < 140$	0.11 (65)	0.04 (73)
$140 < \phi$	0.22 (37)	0.26 (51)

Our calculations of the autocorrelation function yield statistically insignificant correlations for lags of two days or more. However, for a lag of a single day, the correlation values can be large. The one day correlation value is what we are calling persistence. Table 2 presents persistence calculated from the JULIA dataset and sorted by solar flux levels. In this table, the number enclosed in parentheses is the number of observation pairs contributing to the normalized autocorrelation function estimate. The first tabular column represents equinox conditions. We do not possess enough data to make accurate calculations for solstice conditions but have combined what solstice data we do have with the equinox data to compute all-season persistence. The solar flux binning levels used here were chosen so that approximately equal numbers of data would fall into each of the three categories.

Table 2. shows that the persistence of radar plumes approaches 0.4 during solar minimum. Based on persistence alone, one can therefore forecast the occurrence of radar plumes 24 hours in advance during solar minimum equinox with 70% accuracy. (That is, given a persistence of 0.4 and a mean occurrence rate of 50%, the occurrence of spread *F* will mirror the occurrence on the previous day 70% of the time.) For high solar flux conditions, the persistence is lower but still significant. The higher we make the binning threshold that defines high solar flux, the higher the persistence becomes, and we anticipate that the figure will climb as data from higher and higher flux conditions are entered into the JULIA database. Note, however, that the persistence is significantly reduced during moderate solar flux conditions. Persistence forecasting would appear to be ineffective under such conditions, implying a more important role for other forecast methods at such times.

The physical mechanism underlying the apparent one-day memory of the equatorial ionosphere with respect to the occurrence and non-occurrence of radar plumes is not understood. Part of the explanation may involve the role of geomagnetic activity in initiating and suppressing ESF. In the next section of the paper, we will demonstrate a solar flux dependence on the efficiency of geomagnetic forcing of equatorial electrodynamics and of its reversed role during low and high solar flux conditions.

5. Geomagnetic activity

Figure 2 also gives an indication of the relationship between the occurrence of spread *F* in equinox and geomagnetic activity. In this figure, active conditions implies an average value of Kp equal to or in excess of 3 for the six hours preceding the given moment of observation. The effects of geomagnetic activity evidently depend on the solar cycle as well as on local time. Comparison between Figure 2 and Figure 3 hints that these effects depend on season as well. However, we have taken very few data corresponding to geomagnetically active solstice conditions and so will focus our remarks on equinox.

The first row in Figure 2 shows that geomagnetic activity is conducive to irregularity formation prior to midnight during low solar flux conditions and is nearly essential after local midnight. Before midnight, geomagnetic activity causes irregularities to occur more frequently and at considerably higher altitudes than they do otherwise. The effect is even more evident after midnight, when geomagnetic activity causes postmidnight irregularities, which occur infrequently under quiet conditions, to be observed as frequently as they are immediately after sunset.

During moderate solar flux conditions, geomagnetic activity seems to have a much smaller influence on the occurrence of irregularities prior to midnight. Geomagnetic activity meanwhile continues to be nearly essential for the occurrence of post-midnight irregularities. However, the overall rate of occurrence for such irregularities falls drastically with increasing solar flux.

Near solar maximum, geomagnetic activity strongly disrupts spread *F* activity before local midnight. The occurrence of plumes in particular is nearly arrested. After midnight, irregularities continue to be observed during solar maximum during disturbed conditions but at a frequency too low to contribute to Figure 2. For example, strong postmidnight irregularities were observed at June solstice on June 28, 1999 between 4 and 6 LT a few hours following a Kp value of 6. The 10.7 cm solar flux index had reached a value of 207 on June 27.

We note that two classes of irregularities observed after midnight with no close association with geomagnetic activity have been detected by the JULIA radar. One class is composed of echoes sometimes observed briefly just prior to sunrise at altitudes near the *F* peak. These irregularities have been discussed by *Farley et al.* [1970] and *MacDougall et al.* [1998]. Another class is made up of irregularities with small Doppler shifts that that appear to be the remnants of radar plumes that might have formed several hours previously. These may be the signatures of "dead bubbles" [*Aggson et al.*, 1992] and suggest that small-scale waves may continue to be excited by large-scale plasma inhomogeneities long after the primary instability has ceased.

The main features of Figure 2 are in good agreement with the ESF occurrence phenomenology found by *Fejer et al.* [1999] who drew similar conclusions on the basis of Jicamarca incoherent scatter data collected between 1968 and 1992. They explained these features mainly in terms of electric fields driven by the disturbance dynamo process [*Blanc and Richmond*, 1980; *Fejer et al.*, 1983; *Scherliess and Fejer*, 1997]. Disturbance dynamo electric fields result from enhanced energy deposition in the auroral ionosphere during geomagnetically active periods. A modified meridional circulation results which leads to modifications to the dawn-to-dusk electric field observed at mid and low latitudes. The sense of the modification opposes that of the quiet time system and gives rise to ascent (decent) in the late evening (early evening) sectors. The disturbance dynamo is therefore generally stabilizing in the equatorial ionosphere before local midnight and destabilizing thereafter. The post-midnight disturbance dynamo response was found to be independent of solar flux and strongest at about 4 LT. The pre-midnight response was found to have a strong solar flux dependence and is strongest at solar maximum dusk.

Disturbance dynamo electric fields are usually necessary to destabilize the *F* region ionosphere after midnight, which is otherwise stabilized by its low altitude (high collisionality) and by the prevailing westward quiet time electric field. This westward field is easily overcome during solar minimum, where we find a high occurrence of post-midnight irregularities peaking at approximately 4 LT. As the solar flux level increases, so does the amplitude of the westward quiet time field [*Scherliess and Fejer*, 1999]. Thus, stronger and stronger disturbances are required to cause ESF. By solar maximum, post-midnight irregularities become quite rare, but their occurrence is still highly correlated with geomagnetic activity. In contrast, the occurrence of pre-midnight irregularities is strongly anti-correlated with geomagnetic activity at solar maximum. The correlation essentially vanishes during moderate solar flux conditions with the weakening influence of the disturbance dynamo. By solar minimum, the occurrence of pre-midnight irregularities has become correlated with geomagnetic activity, indicating the influence of a mechanism other than the disturbance dynamo. Note that these occurrence patterns reflect observations from Jicamarca and may not hold at other longitudes.

The timescales at which the effects of geomagnetic activity are experienced in the equatorial ionosphere are signatures of the mechanisms at work. Following *Scherliess and Fejer* [1997], we sought to reveal these timescales by correlating our JULIA radar observations with geomagnetic indices. *Scherliess and Fejer* [1997] correlated the departure of measured ionospheric electric fields from their seasonal averaged quiet time values with the AE index, an indicator of convection strength and energy input in the auroral zone. In our case, the variable derived from our dataset is the two-state random variable indicating the occurrence of non-occurrence of a topside plume (see earlier discussion of persistence). We distinguish between plumes observed prior to and after about midnight. Two random variables are then realized once per day.

We correlated these two variables with the PC (polar cap) index, a single station index derived from the magnetometer station at Thule and conceived to measure the degree of IMF merging with the Earth's magnetic field at the magnetopause [*Troshichev et al.*, 1988]. It is calculated from the projection of the total (vector sum) of the horizontal geomagnetic disturbances projected on the dawn-dusk line and is associated with the Hall current in the noon-midnight direction. The PC index has been found to be highly correlated with AE [*Vennerstrøm et al.*, 1991; *Vassiliadis et al.*, 1996; *Takalo and Timonen*, 1998] and has been found to be a good proxy for the hemispheric Joule heating rate [*Chun et al.*, 1999]. PC index values are available at 15 min. intervals and are updated regularly. All of the *F* region data in the JULIA database were used for this analysis.

Figure 4 shows the correlation between the PC index and the observation of plumes before and after 1 LT by the JULIA radar. The former curve is only plotted through 0 LT; to plot the correlation function for later times would be to correlate ESF plumes with future values of PC. Both sets of

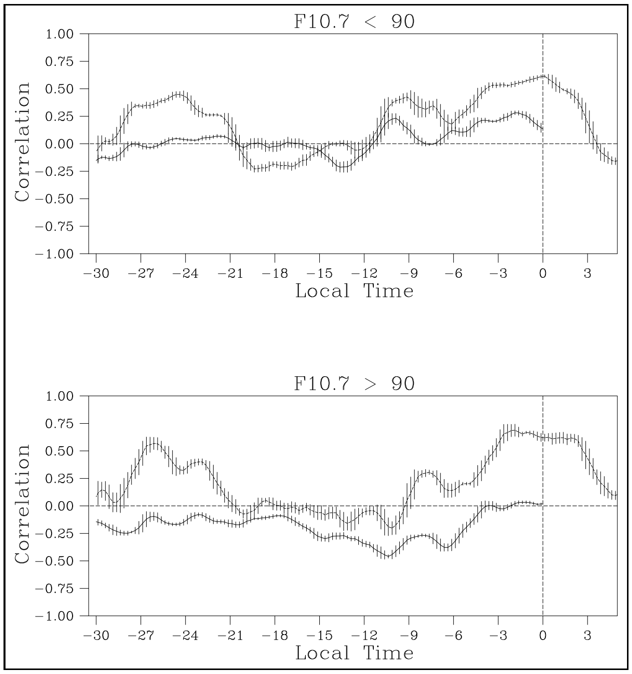

Figure 4. Normalized cross-correlation function between the PC index and the occurrence of pre-midnight (solid lines) and post-midnight (dashed lines) irregularities versus the local time of the PC index. The time index '0' refers to local midnight. One-hour wide sliding window averages have been taken, and the error bars reflect the variance of the averaged values. Correlation functions for low (above) and high (below) solar flux conditions are shown.

curves are calculated for low and high solar flux conditions. Times up though 30 hours prior to local midnight are considered.

Consider first the curves corresponding to radar plumes observed after 1 LT. The curves for low and high solar flux conditions are essentially identical and reveal a strong positive correlation. Two short timescales ($\tau = \sim$1–6 and $\sim$7–12 hours) and a long timescale (τ = 20-30 hours) are clearly evident in the response. This phenomenology is strikingly similar to that found by *Scherliess and Fejer* [1997] even though somewhat different quantities are being considered (note in particular the similarity between these curves and the relative efficiency plotted in Figure 3 of *Scherliess and Fejer* [1997] for 0-4 SLT). *Scherliess and Fejer* [1997] associated the short timescale response of the postmidnight ionosphere to geomagnetic forcing with the disturbance dynamo and found good agreement between equilibration and recovery times resulting from a regression analysis of Jicamarca data and those found by *Fuller-Rowell et al.* [1994]. They meanwhile associated the long timescale response in part with composition changes in the low-latitude ionosphere occurring about 1 day after high-latitude current changes [*Fuller-Rowell et al.*, 1994, 1996].

Turning to the curves in Figure 4 corresponding to radar plumes observed prior to 1 LT, we see totally different behavior for low and high solar flux. During solar maximum conditions, there is a strong anti-correlation with PC values measured from about 5 to 16 hours before local midnight. This timescale too is in good agreement with the response of low-latitude zonal electric fields to geomagnetic activity in solar maximum brought about by the disturbance dynamo [*Scherliess and Fejer*, 1997]. While we might therefore expect to find no correlation during solar minimum, Figure 4 in fact shows a significant positive correlation consistent with the upturn of ESF during solar minimum apparent in Figure 2. This positive correlation is not consistent with the known phenomenology of the disturbance dynamo. Since the correlation is largest between 20 and 24 LT, the time when the radar plumes are actually occurring, the upturn represents a very rapid response to geomagnetic forcing. We are therefore inclined to associate the phenomenon with the prompt penetration of electric fields generated by the solar wind- magnetosphere dynamo [*Senior and Blanc*, 1984].

Fejer and Scherliess [1997] were recently successful in separating empirical evidence for storm-time responses of equatorial electric fields to prompt-penetration and disturbance dynamo effects by taking into account the different impulse responses of the two mechanisms. They showed that, following an increase in the polar cap potential, equatorial electric fields are eastward (westward) during the day (at night) and evolve with a timescale of about 1 hour. The sense of the perturbations is reversed for decreases in the polar cap potential. Sudden decreases in the polar cap potential could therefore destabilize the equatorial ionosphere. Once irregularities develop into the nonlinear regime and radar plumes begin to evolve and ascend to high altitudes, further reversals in the electric field would have little effect on the instabilities. In that sense, the ionosphere functions like a diode with regard to the effect of penetrating electric fields on stability. The effect should and appears to be most pronounced during solar minimum when the quiet-time, westward electric field has a minimum amplitude in the evening.

6. Quiet time variability

Based on the analyses related to the climatology and persistence of ESF irregularities and on their response to magnetic activity, it seems as if an empirical model for forecasting irregularities might easily be constructed. However, the accuracy of the model would suffer from the considerable quiet-time variability exhibited by the zonal ionospheric electric field.

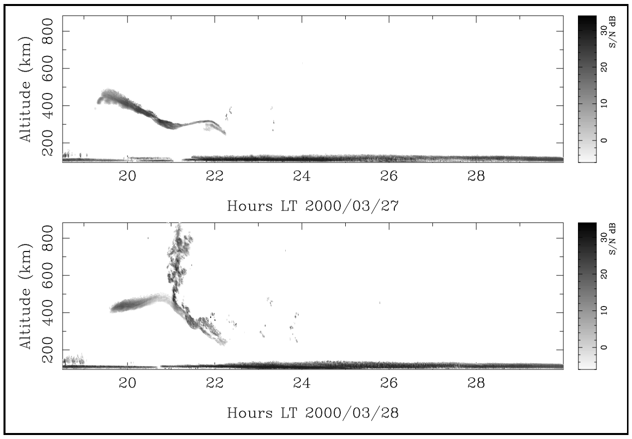

Figure 5. RTI plots for successive days observed by the JULIA radar.

Figure 5 shows RTI plots for two successive days in late March, 2000. The season, solar flux level, and geomagnetic conditions on and preceding these two days were essentially identical. Ionograms for these days (not shown) indicate that the *F* peak at 1930 LT was at approximately 600 km on both days just prior to the onset of coherent backscatter. (The value of f0f2 was approximately 8 MHz on the 27th and 7 MHz on the 28th.) The ionosphere was evidently linearly unstable on both days, and bottom-type layers emerged at nearly the same time and altitude on both days. A forecast model based on linear instability theory might have predicted this. However, whereas the bottom-type later on March 27th descended until being stabilized by collisions, the layer on the 28th ascended, became a bottomside layer, and gave rise to a topside plume at its apex. Variability in the ionospheric electric field evidently contributes substantial variability to ESF.

We have studied the quiet-time variability of the zonal electric field using the JULIA radar. The radar mode utilizes a small antenna with a wide beam to probe plasma irregularities in the electrojet and performs spectral analysis to estimate the ionospheric field from the Doppler shifts of type II echoes. Details about the technique, which was pioneered by *Balsley* [1969], were given by *Hysell and Burcham* [2000]. As an example, Figure 6 shows the estimated zonal electric field for five consecutive days of March, 2000. This period was geomagnetically quiet, but considerable hourly and day-to-day variability is evident. Similar variability in incoherent scatter measurements has been highlighted by *Viswanathan et al.* [1987], *Basu et al.* [1996], and *Scherliess and Fejer* [1999] among others. Gravity waves propagating into the thermosphere are presumed to be the cause.

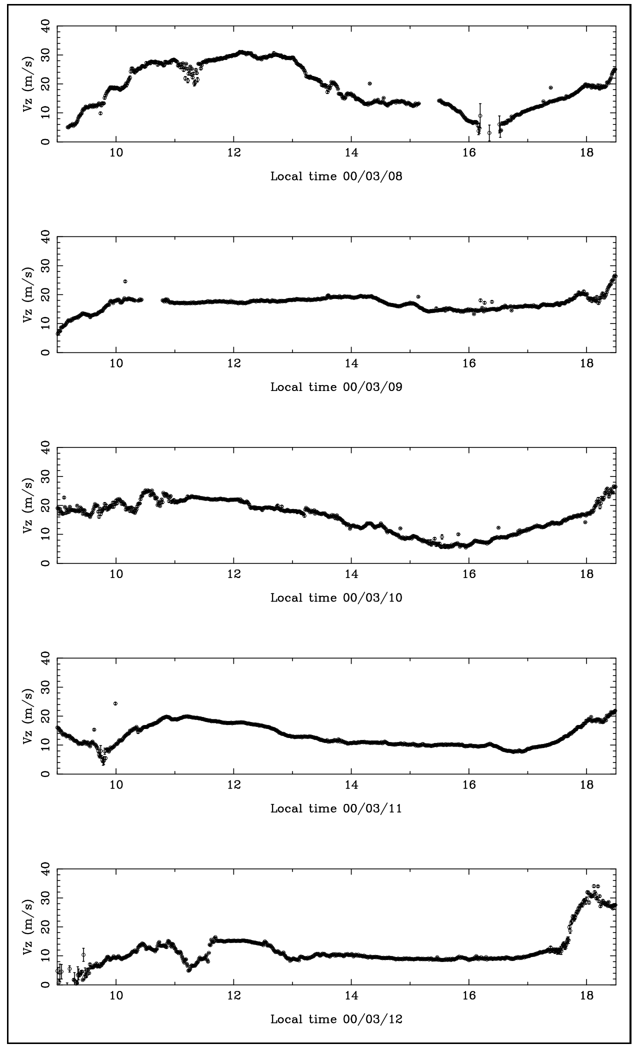

Figure 6. Zonal electric field estimates for five consecutive days of March, 2000. The units are m/s, corresponding to the ExB ascent rates. Statistical error bars are plotted though the points but are generally too small to be discerned. Topside spread *F* was observed only on March 12, the day that also exhibited an early peak in the zonal electric field.

We have attempted to evaluate the effect that the time history of the zonal electric field throughout the afternoon and twilight hours has on “predisposing” the *F* region ionosphere to postsunset instability. Figure 7 shows average electric field estimates from April, 1999 and March, 2000. The 10.7 cm solar flux varied between about 100 and 140 in April, 1999 and 180 and 230 in March, 2000. In the middle and bottom rows, data were sorted according to whether radar plumes were observed at any time after sunset. The two sets of curves show no clear evidence of a systematic difference

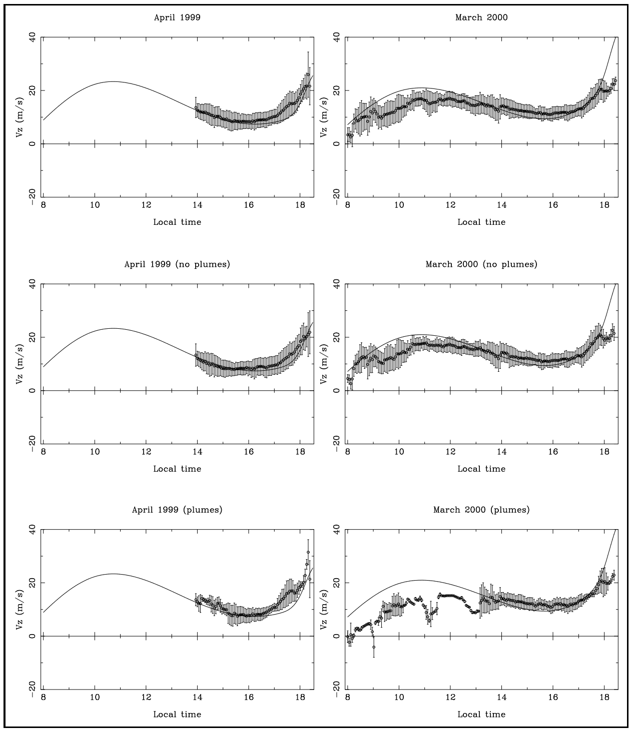

Figure 7. Average electric fields for April, 1999 (left column) and March, 2000 (right column). Solid lines represent quiet time averages derived by *Scherliess and Fejer* [1999] from incoherent scatter data. The top panels represent averages of all available JULIA data. The middle panels represent days when no ESF plumes occurred, and the bottom panels represent days with plumes. Vertical lines drawn through the data points represent geophysical variability and not error bars.

between spread *F* and non-spread *F* nights. Note, however, that our electric field estimates generally start to break down before the time of the peak in the prereversal enhancement. We believe that there will be some predictive benefit in accurately measuring the amplitude and duration of the prereversal enhancement and are attempting to improve our technique to do so. Accurate forecasts made before the time of the prereversal enhancement, though, may well be unobtainable.

7. Summary

In this paper, we have analyzed an extensive archive of radar backscatter data to infer the climatological behavior of ionospheric irregularities in the equatorial *F* region in the Peruvian sector. Irregularity formation is very common except during June solstice, but the most severe spread *F* events, characterized by radar plumes, occur on half of all evenings or less, depending on the solar cycle. As solar flux increases from solar minimum conditions, radar plumes are observed earlier in the evening and at higher altitudes, but they also decay earlier and have an occurrence rate that declines slightly overall. This behavior is consistent with the climatology of the zonal ionospheric electric field. The amplitude of the post reversal electric field is smallest during December solstice, and it is then that we find spread *F* persisting latest into the evening.

Geomagnetic activity affects the occurrence of irregularities in a manner that depends on local time and the season and solar cycle. Disturbance dynamo electric fields appear in the equatorial zone following periods of geomagnetic activity diagnosed by the PC index on intermediate and long timescales. The sense of the disturbance dynamo electric fields is so as to stabilize (destabilize) the equatorial *F* region prior to (after) about local midnight. The post-midnight effect is most evident during solar minimum when the background post-reversal zonal electric field can most easily be overcome by the storm-time perturbations. The pre-midnight response is most evident during solar maximum, when the disturbance dynamo effectively suppresses plume formation. During solar minimum, prompt penetration electric fields give rise to a fast response in the pre-midnight ionosphere, where we find enhanced irregularity formation almost immediately after perturbations appear in the PC index. These findings do not necessary apply to longitude regimes outside the Peruvian sector.

The pre-midnight irregularities under study exhibit significant one-day persistence during low and high solar flux conditions but not under moderate solar fluxes. This phenomenon is not understood but could be another reflection of the effects of geomagnetic activity. During low (high) flux conditions, geomagnetic activity generally enhances (suppresses) irregularity occurrence prior to midnight. Sequential days of unseasonably low (high) spread *F* activity should therefore result following long lived storms. However, during moderate flux conditions, the correlation between geomagnetic activity and irregularity occurrence is weak, as the different mechanisms at work are offset. Consequently, the one-day persistence could be expected to diminish during this time.

Finally, we have discussed the considerable day-to-day quiet time variability in the zonal electric field observed by oblique radar probing of the electrojet. This variability will tend to thwart forecast strategies based on persistence or climatological modeling or on assessments the linear stability of the *F* region at some fixed time. As reported by *Basu et al.* [1996], the peak amplitude of the prereversal enhancement of the zonal electric field is probably highly predictive of irregularity occurrence. We plan to improve our oblique radar technique to attempt to verify this proposition.

Acknowledgments. The authors are thankful for several important discussions with B. G. Fejer. This work was supported by the National Science Foundation through cooperative agreements ATM-9022717 and ATM-9408441 to Cornell University and by NSF grant ATM-9711236 to Clemson University. The Jicamarca Radio Observatory is operated by the Geophysical Institute of Perú, Ministry of Education, with support from the NSF cooperative agreements just mentioned. The help of the staff, particularly R. F. Woodman, J. L. Chau, and M. Sarango, was much appreciated.

References

Aggson, T. L., N. C. Maynard, W. B. Hanson, and J. L. Saba, Electric field observations of equatorial bubbles, *J. Geophys. Res.*, *97*, 2997, 1992.

Balsley, B. B., Measurement of electron drift velocities in the nighttime equatorial electrojet, *J. Atmos. Terr. Phys.*, *31*, 475, 1969.

Basu, S., et al., Scintillations, plasma drifts, and neutral winds in the equatorial ionosphere after sunset, *J. Geophys. Res.*, *101*, 26,795, 1996.

Blanc, M., and A. D. Richmond, The ionospheric disturbance dynamo, *J. Geophys. Res.*, *85*, 1669, 1980.

Chun, F. K., D. J. Knipp, M. G. McHarg, G. Lu, B. A. Emery, S. Vennerstrøm, and O. A. Troshichev, Polar cap index as a proxy for hemispheric Joule heating, *Geophys. Res. Lett.*, *26*, 1101, 1999.

Farley, D. T., B. B. Balsley, R. F. Woodman, and J. P. McClure, Equatorial spread *F*: Implications of VHF radar observations, *J. Geophys. Res.*, *75*, 7199, 1970.

Fejer, B. G., and L. Scherliess, Empirical models of storm-time equatorial zonal electric fields, *J. Geophys. Res.*, *102*, 24,047, 1997.

Fejer, B. G., M. F. Larsen, and D. T. Farley, Equatorial disturbance dynamo electric fields, *Geophys. Res. Lett.*, *10*, 537, 1983.

Fejer, B. G., L. Scherliess, and E. R. de Paula, Effects of the vertical plasma drift velocity on the generation and evolution of equatorial spread *F*, *J. Geophys. Res.*, *104*, 19,859, 1999.

Fuller-Rowell, T. J., M. V. Codrescu, R. J. Moffet, and S. Quegan, Response of the thermosphere and ionosphere to geomagnetic storms, *J. Geophys. Res.*, *99*, 3893, 1994.

Fuller-Rowell, T. J., M. V. Codrescu, H. Rishbeth, R. J. Moffet, and S. Quegan, On the seasonal response of the thermosphere and ionosphere to geomagnetic storms, *J. Geophys. Res.*, *101*, 2343, 1996.

Hysell, D. L., A review and synthesis of plasma irregularities in equatorial spread *F*, *J. Atmos. Sol. Terr. Phys.*, 2000, in press.

Hysell, D. L., and J. Burcham, JULIA radar studies of equatorial spread *F*, *J. Geophys. Res.*, *103*, 29,155, 1998.

Hysell, D. L., and J. Burcham, Ionospheric electric field estimates from radar observations of the equatorial electrojet, *J. Geophys. Res.*, *105*, 2443, 2000.

MacDougall, J. W., M. A. Abdu, P. T. Jayachandran, J. F. Cedile, and I. S. Batista, Presunrise spread *F* at Fortaleza, *J. Geophys. Res.*, *103*, 23,415, 1998.

Scherliess, L., and B. G. Fejer, Storm time dependence of equatorial disturbance dynamo zonal electric fields, *J. Geophys. Res.*, *102*, 24,037, 1997.

Scherliess, L., and B. G. Fejer, Radar and satellite global equatorial *F* region vertical drift model, *J. Geophys. Res.*, *105*, 6829, 1999.

Senior, C., and M. Blanc, On the control of magnetospheric convection by the spatial distribution of ionospheric conductivities, *J. Geophys. Res.*, *89*, 261, 1984.

Takalo, J., and J. Timonen, Comparison of the dynamics of the AU and PC indices, *Geophys. Res. Lett.*, *25*, 2101, 1998.

Troshichev, O. A., V. G. Andressen, S. Vennerstrøm, and E. Friss-Christensen, Magnetic activity in the polar cap: A new index, *Planet. Space Sci.*, *36*, 1095, 1988.

Vassiliadis, S. E., V. Angelopoulos, D. N. Baker, and A. J. Klimas, The relation between the northern polar cap and auroral electrojet geomagnetic indices in the wintertime, *Geophys. Res. Lett.*, *23*, 2781, 1996.

Vennerstrøm, S., E. Friss-Christensen, O. A. Troshichev, and V. G. Andresen, Comparison between the polar cap index, PC, and the auroral electrojet indices AE, AL, and AU, *J. Geophys. Res.*, *96*, 101, 1991.

Viswanathan, K. S., B. T. Vikramkumar, and C. A. Reddy, Electric fields and currents in the equatorial electrojet deduced from VHF radar observations, II, Characteristics of electric fields on quiet and disturbed days, *J. Atmos. Terr. Phys.*, *49*, 193, 1987.

Zargham, S., Numerical simulations of the ionospheric interchange instability, Ph.D. thesis, Cornell Univ., Ithaca, N. Y., 1988.

J. D. Burcham and D. L. Hysell, 205 Kinard Lab, Dept. of Physics and Astronomy, Clemson University, Clemson, SC 29634. (e-mail: dhysell@clemson.edu)